


Thermodynamic stabilization of γ -U–Mo alloys: Effect of Mo content and temperature

Aloïs Castellano, François Bottin, Boris Dorado, and Johann Bouchet
CEA, DAM, DIF, F-91297 Arpajon, France

 (Received 4 February 2020; accepted 22 April 2020; published 15 May 2020)

The γ -U–Mo alloys have been studied by means of *ab initio* molecular-dynamic simulations at 900 K as a function of the Mo concentration (0%, 25%, 50%, 75%, and 100%). Using the temperature-dependent effective potential method with the symmetry-imposed force constant extension, we obtained the vibrational, thermodynamic, and elastic properties of U–Mo, including anharmonicity and disorder. We show that the addition of Mo and temperature effects are responsible for the stabilization of the γ phase of U–Mo alloys in the range of 0–25 % of Mo concentration above 900 K. The vibrational entropy is found to be very large compared to its value in other alloys, about half of the configurational entropy counterpart, and to act against the thermodynamic stabilization of the solid solution. The vibrational and thermodynamic properties are strongly impacted by the disorder, due to the large differences between mass and interatomic bonds of uranium and molybdenum. The increase of elastic shear modulus as a function of the Mo concentration also indicates a mechanical stabilization of the solid solution and validates the thermodynamic findings.

DOI: [10.1103/PhysRevB.101.184111](https://doi.org/10.1103/PhysRevB.101.184111)

I. INTRODUCTION

Metallic uranium based nuclear fuels are promising for next-generation nuclear reactors due to their high thermal conductivity and high density compared to third-generation nuclear fuel. The pure uranium phase diagram is composed of three allotropes: a low-temperature orthorhombic phase α -U, a tetragonal phase β -U, and a high-temperature body-centered-cubic phase γ -U. The cubic symmetry of the γ -U phase allows it to exhibit the best technical properties for nuclear engineering among those three allotropes [1]. Unfortunately, this phase is unstable at low temperature, so that it is usually alloyed with another bcc metal in order to stabilize it. Among those alloys, one of the most promising is the uranium molybdenum alloy.

The phase diagram of U–Mo [2], represented in Fig. 1, has been extensively studied experimentally [3–5] along with thermodynamic assessment [6,7], and recent first-principles studies have focused on its ground state [8–10]. Experimentally, the only stoichiometric compound observed has been U_2Mo , also called γ' , which is stable up to at least 853 K [11]. Below this temperature, and for other concentrations, U–Mo demixes into two phases, with α -U + U_2Mo for Mo content below $\sim 33\%$ and U_2Mo + ϵ -Mo (bcc) for higher molybdenum concentration. At low Mo concentration, the α -U phase undergoes a series of phase transitions as a function of temperature with intermediate β and γ phases of uranium, depending on the Mo concentration [4,12,13]. Between them, a large part of the phase diagram is filled by the γ -U–Mo alloy, which is stable between 0 and 30–40 % of Mo content and over several hundred Kelvin (from 900 to 1500 K, approximately). This is the only region with a solid solution. Note that U–Mo alloys with bcc-like structures can be stabilized at room temperature by quenching high-temperature solid solutions [5,13,14].

Almost all the previous *ab initio* studies have focused on the ground state of U–Mo, with methods such as the coherent potential approximation [9,15], cluster expansion [10,16], or special quasirandom structures [9,17]. They find an asymmetry of the excess ground-state energy with respect to the Mo concentration, in agreement with the large miscibility gap in the U–Mo system. However, the instability of the γ phase at low temperature forbids the use of methods such as density functional perturbation theory (DFPT) to pursue the studies at finite temperature. Therefore, there are currently no finite-temperature first-principles studies of γ -U–Mo in the literature.

To overcome the instability of γ -uranium within the harmonic approximation, one needs to treat anharmonicity non-perturbatively. Recently, several first-principles methods have emerged in the literature to compute thermodynamic properties of strongly anharmonic crystals in a nonperturbative approach. In general, these methods are based on an anharmonic renormalization of the phonon frequencies at the mean-field level. Example of such methods are the stochastic self-consistent harmonic approximation (SSCHA) [18], the self-consistent *ab initio* lattice dynamics (SCAILD) [19], the self-consistent phonon (SCP) [20], or the temperature-dependent effective potential (TDEP) [21]. The last method differs from the others as the renormalization is not self-consistent but is based on *ab initio* molecular dynamics (AIMD), which includes all orders of anharmonicity. Several strongly anharmonic systems have been studied by means of these methods, with promising results [22–25] especially in γ -U [26].

In this work, using a supercell-based method and by means of AIMD, we study how the inclusion of molybdenum in uranium leads to the stabilization of the bcc phase at high temperature. In Sec. II we describe the theoretical background and computational methods. The thermodynamic, elastic, and

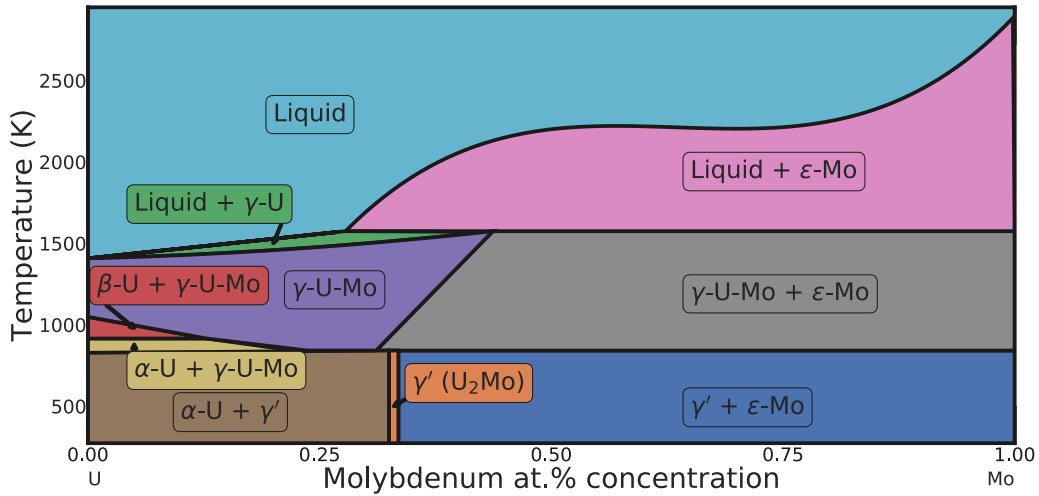


FIG. 1. Phase diagram of U–Mo, adapted from Ref. [2].

vibrational properties of pure γ -U and ϵ -Mo phases as well as of $U_{1-x}Mo_x$ alloys are presented in Sec. III.

II. METHODS

In this section we describe how to take into account the thermodynamic contributions coming from a random alloy. In particular, we show how to compute the configuration and vibrational entropies and to evaluate the finite-temperature properties using an effective temperature-dependent potential. Finally, we describe the computational details used in the simulations.

A. Thermodynamics of random alloys

At constant temperature and pressure, the thermodynamic stability of an alloy is determined by the Gibbs free energy $G = F + PV$. In this paper, we will consider the case of atmospheric pressure, where the PV term is negligible, allowing us to focus on the Helmholtz free energy F . Without magnetic degrees of freedom, we can separate the free energy in three contributions:

$$F = F_{\text{el}} + F_{\text{conf}} + F_{\text{vib}} \quad (1)$$

with F_{el} the electronic, F_{vib} the vibrational, and F_{conf} the configurational contributions, respectively.

Concerning the electronic contribution, the effects of temperature are generally negligible in the stabilization of binary alloys [27] at 900 K. Therefore, the electronic free energy $F_{\text{el}} = U - TS_{\text{el}}$ reduced to the ground-state energy U , which can be computed using density functional theory (DFT) ground-state calculation. In a totally random binary alloy, if we neglect the short-range order, F_{conf} is described by its entropy of configuration $F_{\text{conf}} = -TS_{\text{conf}}$, which reads

$$S_{\text{conf}} = -k_B[(1-x)\ln(1-x) - x\ln(x)] \quad (2)$$

with x the concentration of one of the species, and k_B the Boltzmann constant.

The vibrational contributions account for the vibration of the atoms around their equilibrium positions. In the harmonic

approximation framework, the free energy and entropy are computed using the phonon density of states (DOS) $g(\omega)$ as

$$F_{\text{vib}} = \frac{3N_a}{\beta} \int_0^{\omega_{\text{max}}} \ln \left[2 \sinh \left(\frac{\beta \hbar \omega}{2} \right) \right] g(\omega) d\omega, \quad (3)$$

$$S_{\text{vib}} = 3N_a k_B \int_0^{\omega_{\text{max}}} \left\{ \frac{\beta \hbar \omega}{2} \coth \left(\frac{\beta \hbar \omega}{2} \right) - \ln \left[2 \sinh \left(\frac{\beta \hbar \omega}{2} \right) \right] \right\} g(\omega) d\omega \quad (4)$$

with ω the phonon frequency, ω_{max} the largest phonon frequency, $\beta = \frac{1}{k_B T}$, and N_a the number of atoms in the system.

The thermodynamic stability of a solid solution against demixing is determined with the excess free energy ΔF :

$$\Delta F = F(U_{1-x}Mo_x) - (1-x)F(U) - xF(Mo) \quad (5)$$

with x the Mo content, $F(U_{1-x}Mo_x)$ the free energy of the random alloy at concentration x , and $F(U)$ and $F(Mo)$ the free energy of uranium and molybdenum, respectively. Using the common tangent method, the excess free energy allows us to determine the thermodynamic stability of a random solution. Note that excess entropy ΔS or energy ΔU can be computed in the same way as Eq. (5). In the classical high-temperature limit, the vibrational contribution to the phase stability is mainly due to the vibrational entropy [28].

The temperature effect on the thermodynamic stabilization is driven by the two excess entropy terms ΔS_{conf} and ΔS_{vib} . In the totally random approximation, ΔS_{conf} is positive, which means that ΔF_{conf} always acts in favor of the solid solution stabilization by lowering ΔF . In contrast, the effect of vibrational contribution is less clear (it can be positive or negative), meaning that ΔS_{vib} can either stabilize or destabilize the solid solution [27]. Since ΔS_{vib} is more complex to compute and expected to be lower than ΔS_{conf} , it is often neglected in the computation of the thermodynamic stability of random alloys. However, a typical excess vibrational entropy is around $0.2k_B/\text{at}$, which accounts for about 30% of the configurational entropy [28]. Consequently, the vibrational contribution can have a significant impact on the thermodynamic stability of an alloy [27,29].

B. Temperature-dependent effective potential

In the case of γ -U–Mo, the determination of the vibrational properties is complicated by the dynamical instability of γ -uranium at low temperature. Using the standard harmonic approximation, the phonon band structure of γ -U presents several imaginary soft modes, which prevent us from obtaining the vibrational free-energy contribution using Eq. (3). To describe the vibrational properties of γ -U and its alloys at finite temperature, the intrinsic anharmonic contributions are needed. In this work, we use our own implementation [30] of the temperature-dependent effective potential method [21,31], which has been shown to be effective in the description of γ -U in a previous study [26], and to capture the unusual vibrational properties of α -U at low temperature [32].

In this method, the real potential is mapped onto a temperature-dependent effective potential with a harmonic form such as the model Hamiltonian, which reads

$$\hat{H} = U_0 + \sum_i \frac{p_i^2}{2m_i} + \frac{1}{2} \sum_{ij} \Theta_{ij} \mathbf{u}_i \mathbf{u}_j \quad (6)$$

with m_i , p_i , and \mathbf{u}_i the mass, momentum, and displacement of atom i , respectively. U_0 is the ground-state energy and Θ_{ij} the effective interatomic force constants (IFCs). Using the atomic displacements and forces from the AIMD trajectory, it is possible to extract the effective IFCs by means of a least-squares fitting.

For a supercell with N_a atoms, there are $(3N_a)^2$ coefficients in the IFC matrix. To decrease the computational cost, the number of IFC coefficients is reduced by taking into account the symmetries and invariance of the system. In a $4 \times 4 \times 4$ bcc supercell with 128 atoms (as in the present simulations), this method allows us to reduce the number of IFC coefficients from 147 456 to 13.

In a solid solution, the random distribution of atomic species within the supercell breaks the symmetry of the crystal. In this case, each interaction becomes unique and the previous method cannot be applied in principle. To keep the number of IFC coefficients sufficiently low, several approximations have been proposed. The most crude, named the virtual crystal approximation (VCA) [see Fig. 2(b)], assumes that (i) the underlying symmetry of the supercell is conserved, (ii) the effective IFCs are type-independent, and (iii) the atoms are identical with an averaged mass. If the last assumption is lifted, the system acquires a mass disorder and we obtain the so called “symmetry-imposed force constant molecular dynamics” (SIFC-MD) method proposed by Shulumba and co-workers [33] [see Fig. 2(c)]. On the other hand, if the second hypothesis is also removed, all the bonds become “type-dependent” (SIFC-MDTD) so the effective IFCs are three times more numerous [see Fig. 2(d)]: U–U, Mo–Mo, and U–Mo in the present work. In practice, the effects of IFC-type dependency are generally less important than the effects of mass disorder [34].

Once the IFCs are extracted from the AIMD trajectory, they are mapped on a bigger supercell to ensure convergence with respect to the disorder [see Figs. 2(c) and 2(d)]. To maintain the invariance of the energy with respect to a rigid translation of the crystal, the acoustic sum rule $\sum_{j,\beta} \Phi_{ij}^{\alpha\beta} = 0$ is also imposed on the IFCs during this step. By means of

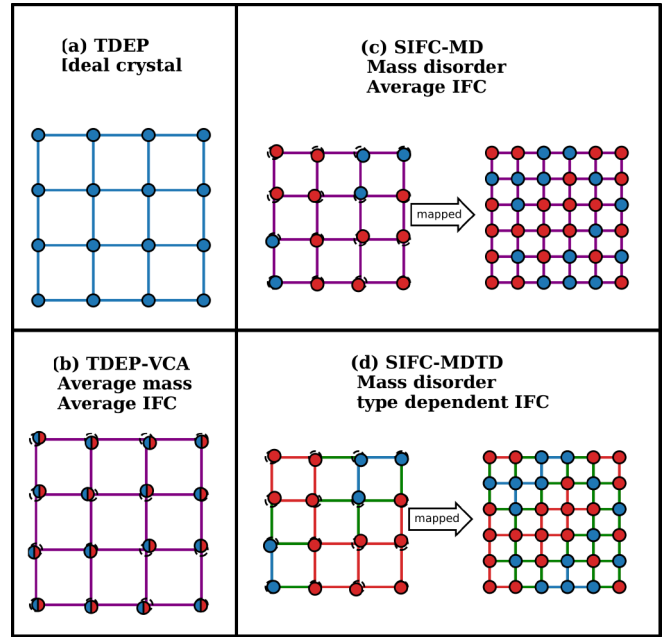


FIG. 2. Schematic representation of the different methods used. The circles and the lines represent the atoms and the interatomic force constants (IFCs), respectively. (a) TDEP for an ideal crystal, (b) TDEP-VCA for an alloy with average mass and IFC, (c) SIFC-MD for an alloy with mass disorder and average IFC, and (d) SIFC-MDTD for an alloy with mass disorder and type-dependent IFC. In (c) and (d), to avoid finite-size effects, the IFCs are mapped onto a bigger supercell.

the full IFC matrix, we can evaluate the vibrational DOS, the free energy within the harmonic approximation, and the elastic constants using the formulation given by Wallace [35] (see Appendix).

C. Computational details

In this work, all the DFT simulations were performed using the ABINIT package [36,37]. Exchange and correlation energy was treated with the generalized gradient approximation (GGA) using the Perdew–Burke–Ernzerhof (PBE) functional [38]. Two projector augmented wave (PAW) [39,40] atomic data for U and Mo were generated using the ATOMPAW code [41,42]. We considered 14 electrons in the valence and a cutoff radius of 2.20 bohr for Mo, and 14 electrons in the valence and a cutoff radius of 2.85 bohr for U, leading to a cutoff energy equal to 544 eV. Since relativistic effects have been shown to impact the γ -U phonon dispersion [43], spin-orbit coupling (SOC) was included.

Concerning the AIMD simulations, we used $4 \times 4 \times 4$ supercells of 128 atoms, and the random alloys were modeled using special quasirandom structure (SQS) [17] generated with ATAT [44] for 25%, 50%, and 75% of Mo content. A $2 \times 2 \times 2$ Monkhorst-Pack \mathbf{k} -point mesh [45] and an AIMD trajectory equilibrated during 5–10 ps are needed to obtain converged IFCs at 900 K. The very long overall time of simulations can be strongly reduced by employing the efficient scheme of parallelization implemented in ABINIT over hundreds up to thousands of processors [46]. For the IFC

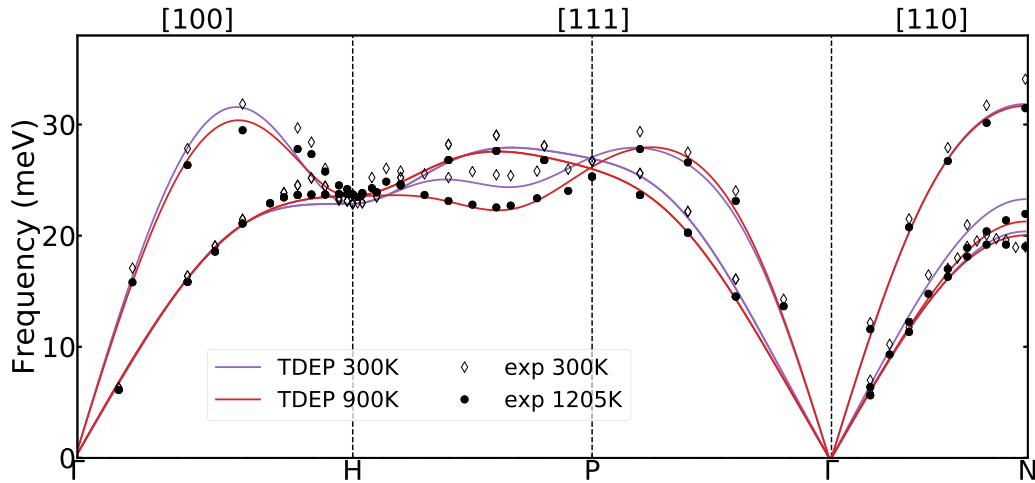


FIG. 3. Phonon band structure of molybdenum at 300 K (purple) and 900 K (red). Experimental results are from [50].

extraction, we used our implementation of the TDEP method [30,32].

Finally, during the SIFC-MD and SIFC-MDTD calculations, the extracted IFCs were mapped onto $8 \times 8 \times 8$ SQS of 1024 atoms. Vibrational thermodynamic properties were computed using PHONOPY [47]. For better stability, the thermodynamic properties were interpolated on the full range of concentrations using cubic splines rather than Redlich-Kister polynomials [48].

III. RESULTS

In this section, we show our results concerning the U–Mo system. We start by describing the phonon spectra of pure molybdenum and uranium, and we compare them with experimental results when available. Then, we describe the thermodynamics of the alloy, first at 0 K and then at 900 K, where we show the effects of vibrational properties and the inclusion of disorder. Finally, we show our results for the mechanical stability of the alloy.

A. Pure elements

1. Molybdenum

Extensive study on the lattice dynamics of molybdenum [49–53] has revealed several anomalies in the phonon dispersion curves, notably a large softening at the H point, and the absence of a dip at the LA 2/3 [111] mode in the H–P direction, generally encountered in bcc structures. The latter have been attributed to bond-bending forces constraining the shearing motion along the 2/3 [111] direction [52]. When increasing temperature, thermal disorder reduces the directional bonding, which in turn allows the appearance of a dip. Concerning the H point softening, several explanations have been given. The more convincing one being the presence of an adiabatic electron-phonon coupling [51]. To capture the electronic origin of those anomalies, the computation of the molybdenum phonon dispersion curves needs a careful convergence of the \mathbf{k} -point grid, and our tests have shown that a $3 \times 3 \times 3$ grid is necessary to obtain a 1 meV convergence

of the free energy at 300 K. At 900 K, the same convergence was observed using only a $2 \times 2 \times 2$ \mathbf{k} -point grid.

We compare in Fig. 3 the phonon dispersion curves computed at 300 and 900 K with experimental results from [50]. We found an overall good agreement between experiment and our theoretical results. The calculations capture the anomalies, notably the soft H-point, as well as the flat nature of the LA 2/3 [111] mode. With temperature we reproduce the anomalous stiffening at the H point. In addition, the softening of phonon branches is also well described when the temperature increases, with a frequency shift comparable to the one obtained in experiments. Nevertheless, slight differences can be observed between experimental and theoretical results. Among them, we find that the softening of a transverse mode at the N point as well as sharp variations around the H point are not described by the theoretical results. To find the origin of those differences, we computed the molybdenum phonon dispersion using DFPT, which reproduces both features. However, if we use the same range of IFCs as in the AIMD supercell, those features disappear and we recover the same dispersion shape as when using TDEP. Furthermore, recent calculations of harmonic phonons in molybdenum using finite differences [54] show similar discrepancies. As the finite differences are a supercell-based method such as TDEP, we conclude that the discrepancies are due to finite-size effects.

2. Uranium

As stated previously, the phonon band structure in γ -U obtained with DFPT presents several soft modes showing the low-temperature instability of the bcc phase. The high-temperature stabilization of this phase has been shown to originate from anharmonic effects [26,43].

The phonon band structure of γ -U computed at 900 K with a $2 \times 2 \times 2$ \mathbf{k} -point mesh (see Fig. 4) is similar to the one obtained in our previous work with the Γ -point only. We can observe that the phonon dispersion does not have any imaginary frequencies, highlighting the dynamical stabilization of the bcc phase at 900 K, even though the transverse mode in the Γ -N direction is relatively soft due to the proximity with the stabilization temperature [26]. One can note that as in

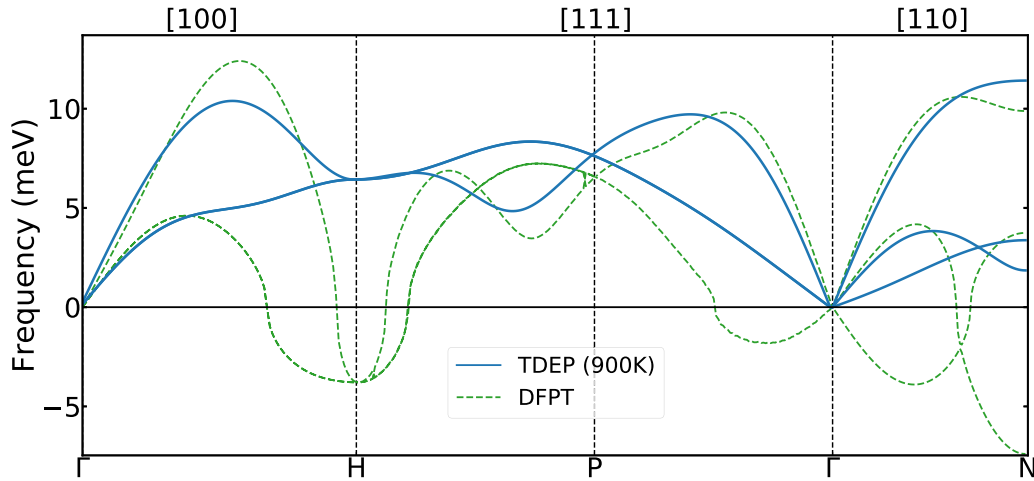


FIG. 4. Phonon band structure of uranium, computed with TDEP at 900 K and DFPT, respectively.

molybdenum, the γ -U phonon dispersion shows a softening located at the H point. Before going forward to the alloy study, we can mention that the uranium phonon frequency range is about one-third of that in molybdenum.

B. The U–Mo alloy

1. Zero temperature

The ground-state energies at different Mo concentrations are obtained through third-order Birch-Murnaghan fit of the total energy versus volume V curves. For each concentration, the atomic positions are left in their high-symmetry positions or relaxed using a Broyden algorithm. In the following, we refer to the former as “unrelaxed” and to the latter as “relaxed.”

In Fig. 5 we compare the results obtained using Eq. (5) with (SOC) or without (NOSOC) the inclusion of spin-orbit

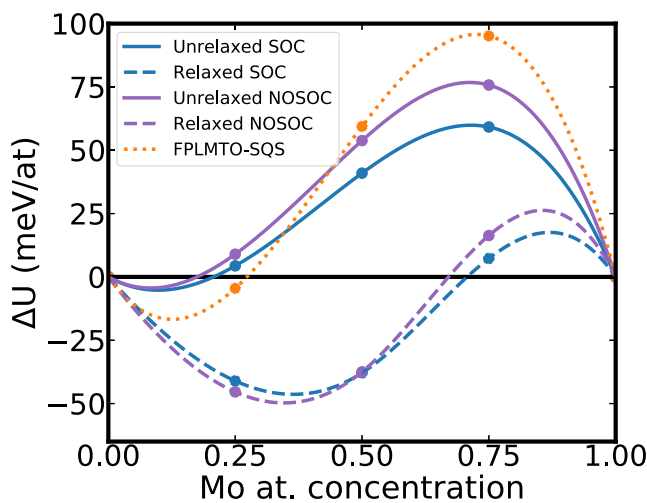


FIG. 5. Evolution of the excess ground-state energy with respect to the molybdenum concentration. The results have been interpolated using cubic spline. The full (dashed) lines are results without (with) relaxation of the SQS, blue (purple) lines are results with (without) inclusion of SOC. FPLMTO-SQS (orange) results are extracted from [9].

coupling. In the unrelaxed case, we found an excess energy consistent with previous results of [9] and [10], with an asymmetry in the excess energy. For low Mo content, ΔU is negative, and a change of sign occurs at $\sim 25\%$ Mo concentration. While results for both NOSOC and SOC are similarly shaped, the inclusion of SOC shifts ΔU toward lower values, this effect being more important in the high Mo concentration range (16 meV for $U_{0.25}Mo_{0.75}$) than in the lower concentration range (4 meV for $U_{0.75}Mo_{0.25}$). The comparison between the present PAW results with the FPLMTO ones [9] shows a qualitative agreement, with the same asymmetric shape for the excess energy but significant differences in amplitudes, in line with what is found for U–Zr [55].

In the relaxed case, the excess energy is significantly shifted to lower values (around 90 meV). Similarly to that obtained in γ -U–Zr [55], we found an overstabilization of the relaxed structure and a strong reduction of the miscibility gap. This behavior comes from the significant displacements of the ions away from the bcc high-symmetry positions. As for γ -U–Zr, we found that the bcc structure is not stable at 0 K, and we will show in the following that temperature stabilizes the bcc structure. In this work, we are interested in the 900 K alloy properties with a stable bcc structure. Consequently, as previously performed by Xie *et al.* [55], we use the unrelaxed reference energies (including SOC) in the following when computing the excess free energies.

2. Finite temperature: 900 K

For each structure, AIMD are performed at 0 K volume. Thus, when computing the free energies, the thermal expansion contribution is neglected. The validity of such an approximation will be discussed later in the text.

Using Eqs. (2) and (4), we plot in Fig. 6 the temperature-dependent part of the excess free energy $-T\Delta S$, with $\Delta S = \Delta S_{\text{conf}} + \Delta S_{\text{vib}}$, for the three different approximations (VCA, SIFC-MD, and SIFC-MDTD) described in Sec. II B. Since we neglected short-range order, the configurational entropy is expressed through the mean field Eq. (2), and its effects on the excess entropy, which is symmetric with respect to the

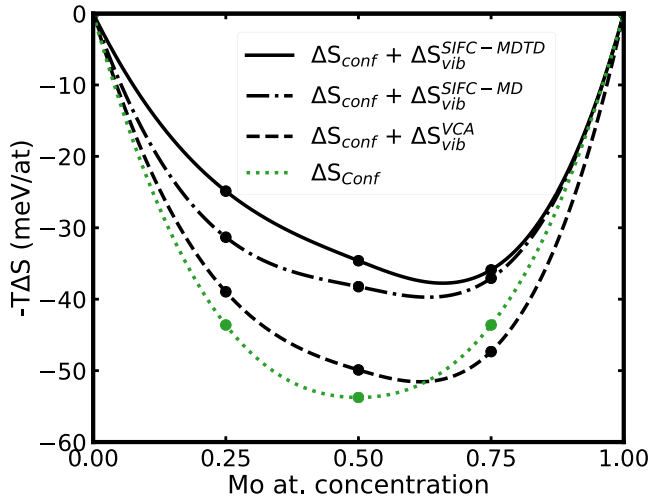


FIG. 6. Evolution of the temperature-dependent part of the excess free energy $-T\Delta S$ with respect to molybdenum concentration at 900 K. The green dashed line corresponds to computation with configurational entropy only. On the black lines, the vibrational entropy is added to the configurational entropy, with the three different approximations (VCA, SIFC-MD, and SIFC-MDTD).

concentration, is always toward thermodynamic stabilization (see the green dotted line in Fig. 6).

When the vibrational entropy is added to the configurational one, the effects of temperature on ΔF are modified, as shown on the black lines of Fig. 6. Within the VCA framework, for which the effects of disorder are neglected, the excess free energy is only slightly modified, with a difference of at most 5 meV compared with configurational entropy-only computation. Moreover, the VCA predicts a diminution of $-T\Delta S$ for high molybdenum concentration ($>60\%$). In contrast, the inclusion of disorder through SIFC approaches creates an overall increase of $-T\Delta S$ over the whole range of concentrations. While both SIFC methods used here show similar changes for high molybdenum content, the additional inclusion of IFC disorder through SIFC-MDTD entails a difference in free energy compared to SIFC-MD for Mo concentration lower than $\sim 60\%$. With SIFC-MD, the difference in $-T\Delta S$ compared to configurational entropy-only computation can go as large as 12 meV, while the type-dependent IFCs in SIFC-MDTD further increase the difference, which gets as large as 19 meV at 25% Mo. Such a difference in the excess free energy can have a significant impact on the temperature of stabilization of the γ phase.

By summing ΔU (see Fig. 5) with $-T\Delta S$ (see Fig. 6) we obtained the excess free energy at 900 K, which is plotted in Fig. 7 and compared to the excess ground-state energy. We obtain an overall shift of the excess free energy toward lower energy between 0 and 900 K, highlighting an increase of the thermodynamic stability and a stabilization of the solid solution as a function of the temperature. Moreover, consistently with the observed miscibility gap, the asymmetry of the free energy is conserved. However, we also note that the excess free-energy shift is limited by an unusually high vibrational contribution. U–Mo is an example of an alloy where vibrational effects are significant ($\Delta S_{\text{vib}} \simeq S_{\text{conf}}/2$). In

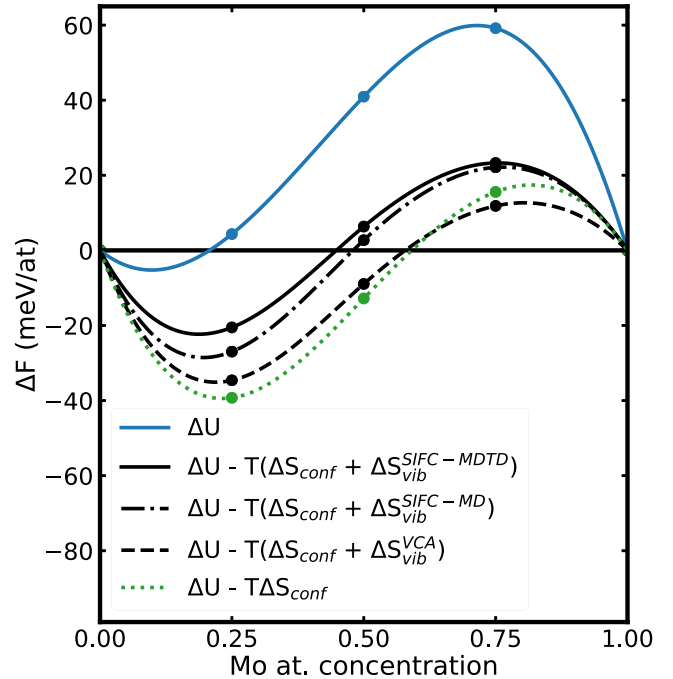


FIG. 7. Evolution of the excess free energy with respect to molybdenum concentration at 900 K, obtained by adding the excess entropy to the excess ground-state energy, including SOC. The green dashed curve corresponds to computation including configurational entropy only. On the black curves, the vibrational entropy is added to the configurational entropy, with the different approximations. The blue curve is the excess ground-state energy from Fig. 5, including SOC.

Ref. [27], the authors review several binary alloys, and among them only $\text{Pt}_{0.8}\text{Ru}_{0.2}$ exhibits such a similar magnitude.

Using the common tangent method, we obtain that the demixing occurs at 28% Mo (ΔS_{conf} only), 26% Mo (VCA), 23% Mo (SIFC-MD), and 22% Mo (SIFC-MDTD) compared to $\sim 33\%$ experimentally [3]. We believe that this discrepancy is mainly due to the neglect of relaxation effects in the high-temperature γ phase, which we cannot take into account due to the instability of U–Mo at 0 K. Moreover, the precision of the common tangent method used to determine the transition concentration can be impacted by the variation of the free-energy curve. Thus, with only five points to extrapolate the excess free energy, the precision of the transition concentration is limited. Nevertheless, the results show clearly the stabilization of the solid solution with temperature, and the limitation of this stabilization by the vibrational contribution.

However, those results do not account for the thermal expansion. To assess the error induced by such an approximation, we use a quasiharmonic model [29] and estimate the correction to the free energy $\Delta^{\text{QH}}F_{\text{vib}}$,

$$\Delta^{\text{QH}}F_{\text{vib}} = -\frac{9}{2}BV_0\alpha^2T^2. \quad (7)$$

In this equation, B is the bulk modulus, V_0 is the volume at which the free energy is computed, and α is the linear thermal

TABLE I. Elastic properties (in GPa) of U–Mo for various concentrations. The values from this work (in bold) are computed using Hill's average with IFC obtained through the SIFC-MDTD method.

Composition	Temperature	Elastic constants				Elastic moduli		
		C_{11}	C_{12}	C_{44}	C'	Bulk	Shear	Young's
U	900 K	118	112	36	3	114	15	43
U (Expt. [59]) ^a						113		
U _{0.80} Mo _{0.20} (Expt. [61]) ^b	Room T	189	163	40	13	172	25	73
U _{0.80} Mo _{0.20} (Expt. [61]) ^c	Room T	179	111	38	34	134	36	100
U _{0.75} Mo _{0.25} (Expt. [60])	Room T					116	34	92
U _{0.75} Mo _{0.25}	900 K	178	147	36	15	157	28	75
U _{0.50} Mo _{0.50}	900 K	241	133	43	54	163	47	127
U _{0.25} Mo _{0.75}	900 K	327	156	57	85	201	67	178
Mo	900 K	373	156	112	109	211	111	286
Mo (Expt. [58])	873 K	428	161	103	136	250	115	300

^aBased on a temperature-independent Birch-Murnaghan fit.

^bComputed from the [100] TA/LA and [011] LA experimental phonon modes.

^cComputed from the [111] TA/LA and [011] LA experimental phonon modes.

expansion coefficient, computed using

$$\alpha = \frac{C_V \gamma}{3BV_0} \quad (8)$$

with C_V the heat capacity and γ the Grüneisen parameter. For the bulk modulus and the specific heat, we use the value obtained using SIFC-MDTD. For the Grüneisen parameter, we use the value of 2.16 of α -uranium, assuming a constant linear thermal expansion coefficient with temperature. This value is greater than the one obtained for γ -U in Ref. [56] using AIMD, allowing us to place a higher bound to $\Delta^{QH}F_{\text{vib}}$. For molybdenum, we use the recommended experimental value of 1.75 from Ref. [57]. Using those parameters, and assuming a relation close to linear in the Mo concentration for γ , we find a correction to the vibrational energy that goes from ~ 8 meV for uranium to ~ 3 meV for molybdenum. Assuming an almost linear evolution of the Grüneisen parameter with Mo content, the correction of the vibrational excess free energy is around 1 meV. Thus, including thermal expansion does not change the conclusions of the present work.

C. Elastic properties

Using the effective IFC, we can compute temperature-dependent elastic properties for the different concentrations. With the three types of approximations, we found similar values for the components of the elastic tensor. This similarity can be attributed to the long-range nature of the elastic properties and their independence from the mass of the atoms in the IFC-based formulation, given in Appendix.

In Table I, we present our results for the different compositions, computed with Hill's formulation and using IFCs from the SIFC-MDTD method, and we compare them to experimental measurements for molybdenum [58], uranium [59], U_{0.75}Mo_{0.25} at 300 K [60], and U_{0.8}Mo_{0.2} at room temperature [61]. For pure uranium, we obtain excellent agreement for the bulk modulus (the only available data) with 114 GPa in the present calculations and 113 GPa in experiments. For pure molybdenum, the agreement is also rather good, except for the C_{11} elastic constant (and thus the bulk modulus),

which is 55 GPa too low in the present calculations. This discrepancy can be attributed to the long-range nature of the elastic constants, requiring large supercells to converge [62].

Concerning the alloys, we found that the increase in molybdenum concentration results in a higher mechanical stability, as shown by an overall increase of the elastic moduli with Mo content. Notably, we found an increase of $C' = (C_{11} - C_{12})/2$, with a value five times higher in U_{0.75}Mo_{0.25} than in γ -U at 900 K. In uranium, the mechanical stabilization of the γ phase is related to the value of C' , which is negative at low temperature [26]. Thus, this increase of C' in U–Mo is a direct observation of the mechanical stabilization of the γ -U bcc phase by molybdenum.

D. Vibrational properties

In a perfect crystal, the harmonic approximation assumes well-defined phonons with given frequencies and eigenvectors. However, the breaking of periodicity due to disorder in an alloy scatters the phonons, which acquire lifetimes, and thus a broadening of the phonon dispersion occurs [34]. Uranium atoms being ~ 2.5 times heavier than molybdenum, we would expect a strong broadening of the phonon DOS in U–Mo.

In Fig. 8 we compare the phonon DOS and projected DOS (pDOS) with various Mo content for the different approximations. The range of frequencies for the phonons in γ -U and ϵ -Mo is completely separated, with molybdenum spanning high frequencies between 14 and 30 meV compared to the 0–12 meV for uranium. As a result, we would expect the solid solutions to contain a separation between the states involving uranium atoms and those involving molybdenum ones.

However, in the VCA, the averaging of the masses and IFCs results in an ideal crystal, and consequently the phonon DOS presents sharp peaks similar to the uranium and molybdenum ones, but with an intermediate-frequency range. The inclusion of mass disorder through SIFC-MD entails the separation of the phonon DOS into two separated and broadened frequency domains: a low-frequency domain dominated by uranium excitations, and a high-frequency one dominated by molybdenum. When introducing type-dependent IFCs with

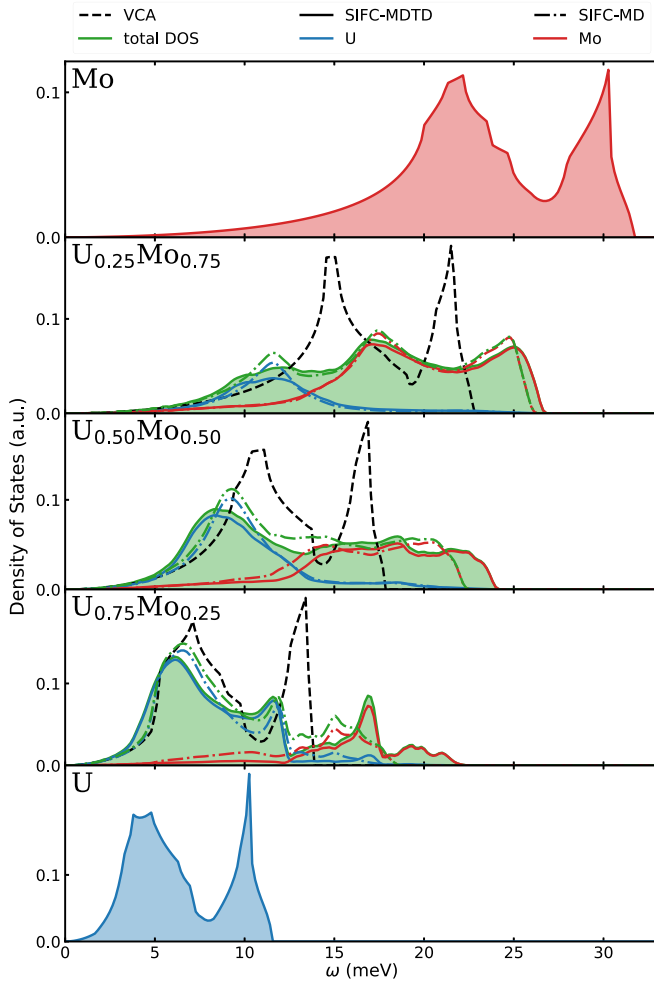


FIG. 8. Phonon DOS and pDOS of $U_{1-x}Mo_x$ at 900 K with VCA (dashed lines), SIFC-MD (dash-dotted lines), and SIFC-MDTD (solid lines). The shaded green area corresponds to the DOS computed with SIFC-MDTD.

SIFC-MDTD, there is a shift in frequencies for the projected DOS compared to SIFC-MD, with the uranium pDOS shifting to lower frequencies while the molybdenum pDOS shifts to higher frequencies. This is particularly visible in $U_{0.75}Mo_{0.25}$, where a gap appears in the DOS, and the highest frequency shifts from 18 to 22 meV, showing that along mass disorder, the force constant disorder affects the vibrational properties of U–Mo.

The broadened double-peak structures of the uranium pDOS for $U_{0.75}Mo_{0.25}$ are consistent with a recent inelastic x-ray scattering measurement on $U_{0.8}Mo_{0.2}$ by Brubaker *et al.* [61], where they observed a bcc-like phonon dispersion with several anomalies and very large lifetimes. We cannot go further in the comparison because their experiments are done at room temperature while the present results are obtained at 900 K. Because the temperature also plays a role in the lifetime broadening, it would be interesting to include both phonon-phonon scattering (not taken into account in these DOS) and alloy disorder scattering in order to carry out a quantitative comparison with experiments at room temperature.

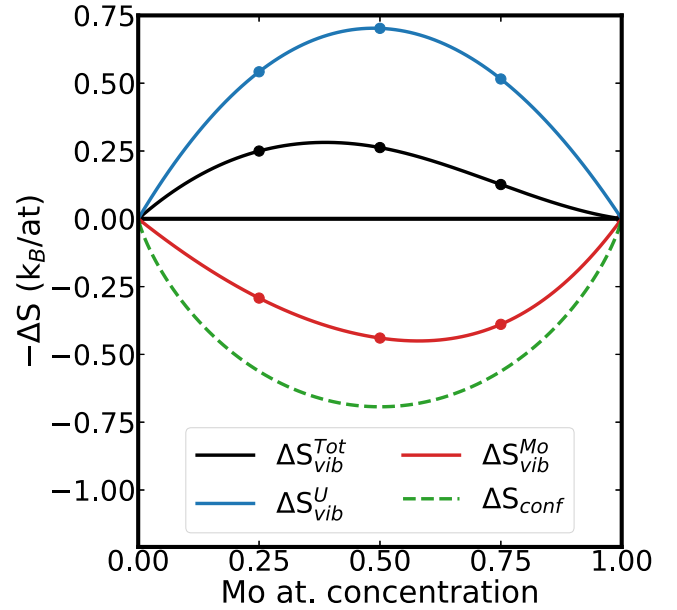


FIG. 9. Evolution of the excess vibrational entropy with respect to molybdenum concentration at 900 K, computed within the SIFC-MDTD method. The configurational entropy is plotted as the green dashed curve for comparison. The blue (red) curve corresponds to the uranium (molybdenum) partial vibrational entropy, and the black curve is the total vibrational entropy.

With the phonon pDOS, the individual contribution of uranium and molybdenum on the vibrational entropy can be computed using Eq. (4), and the corresponding contribution to the excess vibrational entropy can be extracted with Eq. (5). For all molybdenum concentrations, uranium has a negative ΔS_{vib} while molybdenum has a positive ΔS_{vib} , as shown in Fig. 9. However, the amplitude of the contribution of uranium on the excess entropy is higher than that for molybdenum, resulting in negative excess vibrational entropy for the alloy. Thus, the limitation of thermodynamic stabilization by vibrational properties is driven by uranium.

IV. CONCLUSIONS

In this work, we showed that the addition of Mo and temperature effects are responsible for the stabilization of the γ -U phase in the range of 0–25 % Mo concentration at 900 K. By using the temperature-dependent effective potential and its symmetry-imposed force constant extension, we obtained the thermodynamic and elastic properties at 900 K for different Mo concentrations, with good agreement with the few available experimental results in the literature. The effects of disorder were also examined by means of type-dependent IFC and mass disorder through special quasirandom structures.

The various elastic moduli show a strong increase of the mechanical stability of γ -U with respect to the Mo content. In particular, the value of C' goes from 3 to 15 GPa with the addition of 25% Mo at 900 K. The vibrational contribution to the excess free energy was found to be significant in the thermodynamic description of U–Mo and to act against the thermodynamic stabilization of the γ phase at high temperature.

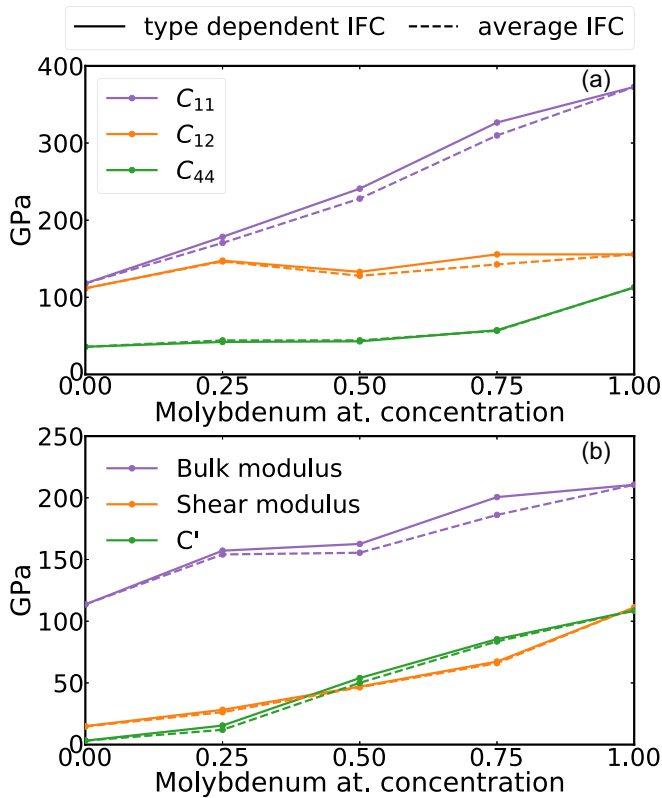


FIG. 10. Evolution of elastic constants (a) and moduli (b) with respect to the molybdenum concentration at 900 K. The continuous lines are the elastic properties computed with the type-dependent IFC, while the dashed lines are computed with the type-independent IFC.

Finally, we plan to perform an additional theoretical study at room temperature in order to evaluate the stability of U–Mo when the solid solution is created after a quench cooling experiment. It would be interesting to understand the structural features of the bcc-like phase and to evaluate the effects of both phonon-phonon scattering and disorder scattering.

ACKNOWLEDGMENTS

The authors would like to thank G. Lander and D. Chaney for fruitful discussions and comments on the manuscript.

APPENDIX: IFC-BASED FORMULATION OF THE ELASTIC PROPERTIES

The elastic properties of a crystal are generally determined by performing finite distortions of the lattice and deriving the elastic constants from the strain-stress relationship. This method has been applied in the case of γ -U [63–65]. While it captures the 0 K instability of the bcc phase with a negative value for C' , the stabilization effect of temperature would need several AIMD simulations to compute the free energies of the strained lattice. To avoid those costly computations, we compute the elastic tensor by using the temperature-dependent IFCs extracted with TDEP.

According to Wallace [35], the elastic constants are defined as

$$C_{\alpha\beta\gamma\delta} = A_{\alpha\gamma\beta\delta} + A_{\beta\gamma\alpha\delta} - A_{\alpha\beta\gamma\delta}, \quad (\text{A1})$$

where $A_{\alpha\beta\gamma\delta}$ are defined with the IFC through

$$A_{\alpha\beta\gamma\delta} = \frac{1}{2V} \sum_{ij} \Phi_{ij}^{\alpha\beta} d_{ij}^{\gamma} d_{ij}^{\delta}. \quad (\text{A2})$$

In Eqs. (A1) and (A2), $\alpha, \beta, \gamma,$ and δ are space coordinates, V is the volume, d_{ij}^{γ} is the distance between atoms i and j in the γ direction, and $\Phi_{ij}^{\alpha\beta}$ is the IFC relating the displacement in the α direction of atom i with the displacement in the β direction of atom j . The elastic tensor can be reduced using Voigt notation, and several elastic properties such as those shown in Table I can be computed with it. However, we note that the main drawback of this method is that the long-range nature of the elastic properties require a large supercell to converge the sum in Eq. (A2).

One can also note that the elastic constants do not depend on the method used. On the one hand, the mass of the atoms does not appear in Eqs. (A1) and (A2), therefore the elastic properties computed within the VCA and the SIFC-MD method are identical. On the other hand, the fluctuations of IFC are canceled for long wavelength, so elastic constants computed using VCA or SIFC-MD are almost identical with a maximum difference of 7% between them (see Fig. 10).

- [1] V. V. Kalashnikov, V. V. Titova, G. I. Sergeev, and A. G. Samoilov, Uranium-molybdenum alloys in reactor construction, *At. Energy* **5**, 1315 (1959).
- [2] H. Okamoto, Mo-U (molybdenum-uranium), *J. Phase Equilib. Diffus.* **33**, 497 (2012).
- [3] A. E. Dwight, The uranium-molybdenum equilibrium diagram below 900 c, *J. Nucl. Mater.* **2**, 81 (1960).
- [4] K. Tangri and G. Williams, Metastable phases in the uranium molybdenum system and their origin, *J. Nucl. Mater.* **4**, 226 (1961).
- [5] V. Sinha, P. Hegde, G. Prasad, G. Dey, and H. Kamath, Phase transformation of metastable cubic γ -phase in UMo alloys, *J. Alloy Compd.* **506**, 253 (2010).
- [6] A. Berche, N. Dupin, C. Guéneau, C. Rado, B. Sundman, and J. Dumas, Calphad thermodynamic description of some binary systems involving U, *J. Nucl. Mater.* **411**, 131 (2011).
- [7] X. Zhang, Y. Cui, G. Xu, W. Zhu, H. Liu, B. Yin, and Z. Jin, Thermodynamic assessment of the U–Mo–Al system, *J. Nucl. Mater.* **402**, 15 (2010).
- [8] E. Losada and J. Garcés, On the ground state of the U–Mo system, *J. Nucl. Mater.* **518**, 380 (2019).
- [9] A. Landa, P. Söderlind, and P. Turchi, Density-functional study of U–Mo and U–Zr alloys, *J. Nucl. Mater.* **414**, 132 (2011).
- [10] P. R. Alonso and G. H. Rubiolo, The role of multisite interactions in the formation energy of bcc γ (U, Mo) disordered phase, *Model. Simul. Mater. Sci. Eng.* **15**, 263 (2007).

- [11] T. Kutty, S. Dash, J. Banerjee, S. Kaity, A. Kumar, and C. Basak, Thermophysical properties of U₂Mo intermetallic, *J. Nucl. Mater.* **420**, 193 (2012).
- [12] B. Howlett, A study of the shear transformations from the gamma-phase in uranium-molybdenum alloys containing 6.0–12.5 at % molybdenum, *J. Nucl. Mater.* **35**, 278 (1970).
- [13] H. L. Yakel, Crystal structures of transition phases formed in U/16.60 at% Nb/5.64 at% Zr alloys, *J. Nucl. Mater.* **33**, 286 (1969).
- [14] V. Sinha, P. Hegde, G. Prasad, G. Dey, and H. Kamath, Effect of molybdenum addition on metastability of cubic γ -uranium, *J. Alloy Compd.* **491**, 753 (2010).
- [15] L. Vitos, I. A. Abrikosov, and B. Johansson, Anisotropic Lattice Distortions in Random Alloys from First-Principles Theory, *Phys. Rev. Lett.* **87**, 156401 (2001).
- [16] J. Sanchez, F. Ducastelle, and D. Gratias, Generalized cluster description of multicomponent systems, *Physica A* **128**, 334 (1984).
- [17] A. Zunger, S.-H. Wei, L. G. Ferreira, and J. E. Bernard, Special Quasirandom Structures, *Phys. Rev. Lett.* **65**, 353 (1990).
- [18] R. Bianco, I. Errea, L. Paulatto, M. Calandra, and F. Mauri, Second-order structural phase transitions, free energy curvature, and temperature-dependent anharmonic phonons in the self-consistent harmonic approximation: Theory and stochastic implementation, *Phys. Rev. B* **96**, 014111 (2017).
- [19] P. Souvatzis, O. Eriksson, M. I. Katsnelson, and S. P. Rudin, Entropy Driven Stabilization of Energetically Unstable Crystal Structures Explained from First Principles Theory, *Phys. Rev. Lett.* **100**, 095901 (2008).
- [20] T. Tadano and S. Tsuneyuki, First-principles lattice dynamics method for strongly anharmonic crystals, *J. Phys. Soc. Jpn.* **87**, 041015 (2018).
- [21] O. Hellman, P. Steneteg, I. A. Abrikosov, and S. I. Simak, Temperature dependent effective potential method for accurate free energy calculations of solids, *Phys. Rev. B* **87**, 104111 (2013).
- [22] T. Tadano and S. Tsuneyuki, Self-consistent phonon calculations of lattice dynamical properties in cubic SrTiO₃ with first-principles anharmonic force constants, *Phys. Rev. B* **92**, 054301 (2015).
- [23] J. Bouchet, F. Bottin, V. Recoules, F. Remus, G. Morard, R. M. Bolis, and A. Benuzzi-Mounaix, *Ab initio* calculations of the B1-B2 phase transition in MgO, *Phys. Rev. B* **99**, 094113 (2019).
- [24] I. Errea, M. Calandra, and F. Mauri, Anharmonic free energies and phonon dispersions from the stochastic self-consistent harmonic approximation: Application to platinum and palladium hydrides, *Phys. Rev. B* **89**, 064302 (2014).
- [25] P. Souvatzis, S. Arapan, O. Eriksson, and M. I. Katsnelson, Temperature-driven α -to- β phase transformation in Ti, Zr and Hf from first-principles theory combined with lattice dynamics, *Europhys. Lett.* **96**, 66006 (2011).
- [26] J. Bouchet and F. Bottin, High-temperature and high-pressure phase transitions in uranium, *Phys. Rev. B* **95**, 054113 (2017).
- [27] A. Manzoor, S. Pandey, D. Chakraborty, S. R. Phillpot, and D. S. Aidhy, Entropy contributions to phase stability in binary random solid solutions, *npj Comput. Mater.* **4**, 47 (2018).
- [28] A. van de Walle and G. Ceder, The effect of lattice vibrations on substitutional alloy thermodynamics, *Rev. Mod. Phys.* **74**, 11 (2002).
- [29] B. Fultz, Vibrational thermodynamics of materials, *Prog. Mater. Sci.* **55**, 247 (2010).
- [30] F. Bottin, J. Bieder, and J. Bouchet, a-TDEP: Temperature dependent effective potential for abinit-lattice dynamic properties including anharmonicity, *Comput. Phys. Commun.* **107301** (2020), doi: [10.1016/j.cpc.2020.107301](https://doi.org/10.1016/j.cpc.2020.107301).
- [31] O. Hellman, I. A. Abrikosov, and S. I. Simak, Lattice dynamics of anharmonic solids from first principles, *Phys. Rev. B* **84**, 180301(R) (2011).
- [32] J. Bouchet and F. Bottin, Thermal evolution of vibrational properties of α -U, *Phys. Rev. B* **92**, 174108 (2015).
- [33] N. Shulumba, O. Hellman, Z. Raza, B. Alling, J. Barrirero, F. Mücklich, I. A. Abrikosov, and M. Odén, Lattice Vibrations Change the Solid Solubility of an Alloy at High Temperatures, *Phys. Rev. Lett.* **117**, 205502 (2016).
- [34] F. Körmann, Y. Ikeda, B. Grabowski, and M. H. F. Sluiter, Phonon broadening in high entropy alloys, *npj Comput. Mater.* **3**, 36 (2017).
- [35] D. C. Wallace, *Statistical Physics of Crystals and Liquids: A Guide to Highly Accurate Equations of State* (World Scientific, Singapore, 2002).
- [36] X. Gonze, F. Jollet, F. A. Araujo, D. Adams, B. Amadon, T. Applencourt, C. Audouze, J.-M. Beuken, J. Bieder, A. Bokhanchuk, E. Bousquet, F. Bruneval, D. Caliste, M. Côté, F. Dahm, F. D. Pieve, M. Delaveau, M. D. Gennaro, B. Dorado, C. Espejo, G. Geneste, L. Genovese, A. Gerossier, M. Giantomassi, Y. Gillet, D. Hamann, L. He, G. Jomard, J. L. Janssen, S. L. Roux, A. Levitt, A. Lherbier, F. Liu, I. Lukačević, A. Martin, C. Martins, M. Oliveira, S. Poncé, Y. Pouillon, T. Rangel, G.-M. Rignanese, A. Romero, B. Rousseau, O. Rubel, A. Shukri, M. Stankovski, M. Torrent, M. V. Setten, B. V. Troeye, M. Verstraete, D. Waroquiers, J. Wiktor, B. Xu, A. Zhou, and J. Zwanziger, Recent developments in the ABINIT software package, *Comput. Phys. Commun.* **205**, 106 (2016).
- [37] X. Gonze, B. Amadon, G. Antonius, F. Arnardi, L. Baguet, J.-M. Beuken, J. Bieder, F. Bottin, J. Bouchet, E. Bousquet, N. Brouwer, F. Bruneval, G. Brunin, T. Cavnac, J.-B. Charraud, W. Chen, M. Côté, S. Cottenier, J. Denier, G. Geneste, P. Ghosez, M. Giantomassi, Y. Gillet, O. Gingras, D. R. Hamann, G. Hautier, X. He, N. Helbig, N. Holzwarth, Y. Jia, F. Jollet, W. Lafargue-Dit-Hauret, K. Lejaeghere, M. A. Marques, A. Martin, C. Martins, H. P. Miranda, F. Naccarato, K. Persson, G. Petretto, V. Planes, Y. Pouillon, S. Prokhorenko, F. Ricci, G.-M. Rignanese, A. H. Romero, M. M. Schmitt, M. Torrent, M. J. van Setten, B. V. Troeye, M. J. Verstraete, G. Zérah, and J. W. Zwanziger, The abinitproject: Impact, environment and recent developments, *Comput. Phys. Commun.* **248**, 107042 (2020).
- [38] J. P. Perdew, K. Burke, and M. Ernzerhof, Generalized Gradient Approximation Made Simple, *Phys. Rev. Lett.* **77**, 3865 (1996).
- [39] P. E. Blöchl, Projector augmented-wave method, *Phys. Rev. B* **50**, 17953 (1994).
- [40] M. Torrent, F. Jollet, F. Bottin, G. Zérah, and X. Gonze, Implementation of the projector augmented-wave method in the ABINIT code: Application to the study of iron under pressure, *Comput. Mater. Sci.* **42**, 337 (2008).
- [41] N. Holzwarth, A. Tackett, and G. Matthews, A projector augmented wave (PAW) code for electronic structure calculations, Part I: atompaw for generating atom-centered functions, *Comput. Phys. Commun.* **135**, 329 (2001).

- [42] F. Jollet, M. Torrent, and N. Holzwarth, Generation of projector augmented-wave atomic data: A 71 element validated table in the XML format, *Comput. Phys. Commun.* **185**, 1246 (2014).
- [43] P. Söderlind, B. Grabowski, L. Yang, A. Landa, T. Björkman, P. Souvatzis, and O. Eriksson, High-temperature phonon stabilization of γ -uranium from relativistic first-principles theory, *Phys. Rev. B* **85**, 060301(R) (2012).
- [44] A. van de Walle, P. Tiwary, M. de Jong, D. Olmsted, M. Asta, A. Dick, D. Shin, Y. Wang, L.-Q. Chen, and Z.-K. Liu, Efficient stochastic generation of special quasirandom structures, *Calphad* **42**, 13 (2013).
- [45] H. J. Monkhorst and J. D. Pack, Special points for Brillouin-zone integrations, *Phys. Rev. B* **13**, 5188 (1976).
- [46] F. Bottin, S. Leroux, A. Knyazev, and G. Zérah, Large-scale *ab initio* calculations based on three levels of parallelization, *Comput. Mater. Sci.* **42**, 329 (2008).
- [47] A. Togo and I. Tanaka, First principles phonon calculations in materials science, *Scr. Mater.* **108**, 1 (2015).
- [48] G. H. Teichert, N. H. Gunda, S. Rudraraju, A. R. Natarajan, B. Puchala, K. Garikipati, and A. V. der Ven, A comparison of redlich-kister polynomial and cubic spline representations of the chemical potential in phase field computations, *Comput. Mater. Sci.* **128**, 127 (2017).
- [49] Y. Wang, R. Ahuja, O. Eriksson, B. Johansson, and G. Grimvall, Precise solution for h-point oscillation: Mo, Na, and Fe, *J. Phys. Condens. Matter* **14**, L453 (2002).
- [50] J. Zarestky, C. Stassis, B. N. Harmon, K. M. Ho, and C. L. Fu, Temperature dependence of the vibrational modes of molybdenum, *Phys. Rev. B* **28**, 697 (1983).
- [51] D. L. Farber, M. Krisch, D. Antonangeli, A. Beraud, J. Badro, F. Occelli, and D. Orlikowski, Lattice Dynamics of Molybdenum at High Pressure, *Phys. Rev. Lett.* **96**, 115502 (2006).
- [52] K.-M. Ho, C. L. Fu, and B. N. Harmon, Vibrational frequencies via total-energy calculations. Applications to transition metals, *Phys. Rev. B* **29**, 1575 (1984).
- [53] C. M. Varma and W. Weber, Phonon dispersion in transition metals, *Phys. Rev. B* **19**, 6142 (1979).
- [54] Y. Lysogorskiy, T. Hammerschmidt, J. Janssen, J. Neugebauer, and R. Drautz, Transferability of interatomic potentials for molybdenum and silicon, *Model. Simul. Mater. Sci. Eng.* **27**, 025007 (2019).
- [55] W. Xie, W. Xiong, C. A. Marianetti, and D. Morgan, Correlation and relativistic effects in U metal and U-Zr alloy: Validation of *ab initio* approaches, *Phys. Rev. B* **88**, 235128 (2013).
- [56] R. Q. Hood, L. H. Yang, and J. A. Moriarty, Quantum molecular dynamics simulations of uranium at high pressure and temperature, *Phys. Rev. B* **78**, 024116 (2008).
- [57] Y. Zhao, A. C. Lawson, J. Zhang, B. I. Bennett, and R. B. Von Dreele, Thermoelastic equation of state of molybdenum, *Phys. Rev. B* **62**, 8766 (2000).
- [58] J. M. Dickinson and P. E. Armstrong, Temperature dependence of the elastic constants of molybdenum, *J. Appl. Phys.* **38**, 602 (1967).
- [59] C.-S. Yoo, H. Cynn, and P. Söderlind, Phase diagram of uranium at high pressures and temperatures, *Phys. Rev. B* **57**, 10359 (1998).
- [60] M. B. Waldron, R. S. Burnett, and S. F. Pugh, *The Mechanical Properties of Uranium-Molybdenum Alloys* (UK Atomic Energy Authority, United Kingdom, 1958).
- [61] Z. E. Brubaker, S. Ran, A. H. Said, M. E. Manley, P. Söderlind, D. Rosas, Y. Idell, R. J. Zieve, N. P. Butch, and J. R. Jeffries, Phonon dispersion of Mo-stabilized γ -U measured using inelastic x-ray scattering, *Phys. Rev. B* **100**, 094311 (2019).
- [62] I. Schnell, M. D. Jones, S. P. Rudin, and R. C. Albers, Tight-binding calculations of the elastic constants and phonons of hcp-Zr: Complications due to anisotropic stress and long-range forces, *Phys. Rev. B* **74**, 054104 (2006).
- [63] B. Beeler, C. Deo, M. Baskes, and M. Okuniewski, First principles calculations of the structure and elastic constants of α , β and γ uranium, *J. Nucl. Mater.* **433**, 143 (2013).
- [64] C. D. Taylor, Evaluation of first-principles techniques for obtaining materials parameters of α -uranium and the (001) α -uranium surface, *Phys. Rev. B* **77**, 094119 (2008).
- [65] S. Shang, A. Saengdeejing, Z. Mei, D. Kim, H. Zhang, S. Ganeshan, Y. Wang, and Z. Liu, First-principles calculations of pure elements: Equations of state and elastic stiffness constants, *Comput. Mater. Sci.* **48**, 813 (2010).